# Journal of Materials Chemistry A

Accepted Manuscript


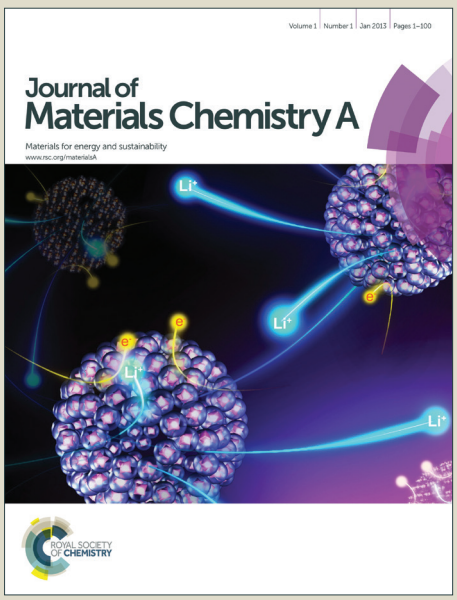





ROYAL SOCIETY OF CHEMISTRY

www.rsc.org/materialsA

Journal Name

RSCPublishing

COMMUNICATION

# Self-assembled three-dimensional hierarchical porous $V_2O_5$/graphene hybrid aerogels for supercapacitors with high energy density and long cycle life

Cite this: DOI: 10.1039/x0xx00000x

Received 00th January 2012,
Accepted 00th January 2012

DOI: 10.1039/x0xx00000x

www.rsc.org/

Yingjie Wu, Guohua Gao* and Guangming Wu*

**This paper describes the synthesis of hierarchical porous vanadium pentoxide ($V_2O_5$)/graphene hybrid aerogel through a low-cost and facile sol-gel method. The $V_2O_5$/graphene hybrid aerogel is synthesized through the *in-situ* growth of $V_2O_5$ nanofibers on graphene sheets. The $V_2O_5$/graphene hybrid aerogel-based supercapacitors exhibit enhanced specific capacitance (486 F $g^{-1}$), high energy density (68 Wh $kg^{-1}$) and outstanding cycle performance. These effects are attributed to the unique hierarchical porous structure of the hybrid aerogel.**

Supercapacitors, which are also called electrochemical capacitors or ultracapacitors, bridge the gap between batteries and conventional solid-state and electrolytic capacitors because these supercapacitors exhibit high power density, superior rate capability, rapid charging/discharging rate, long operating lifetimes, and low maintenance cost.[1, 2] However, the energy density of supercapacitors is significantly lower than batteries and fuel cells.[3] The energy density (E) of a supercapacitor is governed by the specific capacitance (C) and cell potential (V) of a supercapacitor according to the equation $E = 1/2CV^2$.[4] Thus, supercapacitors should enhance specific capacitance, which largely depends on the specific surface area of electrode materials.[5] Supercapacitors based on aerogels, especially carbonaceous aerogels (*e.g.* carbon, carbon nanotube, and graphene aerogels), exhibit a specific capacitance of 128 F $g^{-1}$; this high specific capacitance is attributed to the unique three-dimensional (3D) porous structure, low density, high conductivity, and large specific surface area of carbonaceous aerogels.[6–11] Metal oxide/carbon hybrid aerogels have recently attracted considerable attention because these metal oxide/carbon hybrid aerogels exhibit composite structure of electrochemical double layer capacitors (EDLCs) and pseudocapacitors; these metal oxide/carbon hybrid aerogels exhibit higher capacitance than carbon-based supercapacitors, such as manganese oxide/carbon aerogel microbead composite (368 F $g^{-1}$),[12] nickel oxide/carbon aerogel composite (356 F $g^{-1}$),[13] tin oxide/graphene (310 F $g^{-1}$),[14] and manganese oxide/graphene hybrid aerogel (242 F $g^{-1}$)[15].

Composite aerogels are generally prepared by fabricating 3D aerogel skeletons and depositing or adsorbing active materials.[8, 16, 17] Hydrothermal process is another feasible pathway of preparing composite aerogels; in this technique, a 3D framework structure of aerogel forms and combines with active materials.[18–20] However, these methods exhibit poor compatibility and weak interaction between modified materials and aerogel substrates. A nonhomogeneous and unstable structure seriously affects electrochemical performance of supercapacitors.[18] To date, producing functional aerogel electrode materials for supercapacitors through appropriate routes remain a challenge.

This paper reports a mild and facile one-pot sol–gel process to synthesize 3D $V_2O_5$/graphene hybrid aerogel ($V_2O_5$/GN-Ae) by *in-situ* self-assembly of $V_2O_5$ nanofibers and graphene sheets for the first time. The $V_2O_5$/GN-Ae exhibits 3D hierarchical porous structure, good mechanical strength, and stable pore geometry and pore size. The hybrid aerogel-based supercapacitors demonstrate enhanced specific capacitance, high power and energy densities, and excellent cycle stability. These properties are attributed to the synergistic effect of the EDLCs (graphene) and the pseudocapacitors ($V_2O_5$). Moreover, the $V_2O_5$/GN-Ae aerogels do not require harsh

conditions during fabrication compared with common aerogel composites. Thus, the $V_2O_5$/GN-Ae aerogels are easily controlled and mass produced.

Fig. 1 shows the preparation and structure of the $V_2O_5$/graphene hybrid aerogel. First, we prepared a functionalized $V_2O_5$ sol from a relatively cheap commercial $V_2O_5$ powder. Cheap $V_2O_5$ powder was used to avoid the use of costly vanadium precursors (*e.g.* vanadium oxytripropoxide and metavanadate) (Experimental Section in ESI†). The as-prepared light yellow sol was composed of vanadium oxide ($VO_x$) oligomers; Scheme S1† shows the possible chemical reaction pathway in producing $V_2O_5$ sol.[21–23] Graphene oxide (GO) aqueous solution was then added in the $V_2O_5$ sol under vigorous stirring to induce hydrolysis and *in-situ* recombination of the GO sheets and the $VO_x$ oligomers. A dark red $VO_x$/GO hybrid gel was obtained after about 5 min because of the rapid formation of vanadium intermediate phases and growth of nanofibers. The gel was aged for 2 day,[24] and the gel gradually changed to a deep green hydrogel ($VO_x$/GO-Hy), which indicated the presence of $V^{4+}$.[25] The $VO_x$/GO hybrid aerogel ($VO_x$/GO-Ae) was obtained after solvent replacement, and supercritical $CO_2$ drying or freeze drying was performed. Shrinkage was not observed during the drying process because of the stable skeleton structure of the 3D architecture. The as-prepared aerogel was then annealed in air at 300 °C to thermally reduce the GO.[26] The $V^{4+}$ ion was oxidized to $V^{5+}$, and the $V_2O_5$ partly crystallized during thermal treatment (Fig. S1†). These processes occurred simultaneously. Finally, the yellow $V_2O_5$/graphene hybrid aerogel was successfully obtained. For comparison, the $VO_x$ aerogel ($VO_x$-Ae) and the $V_2O_5$ aerogel ($V_2O_5$-Ae) were also obtained under the same conditions but absence of GO.

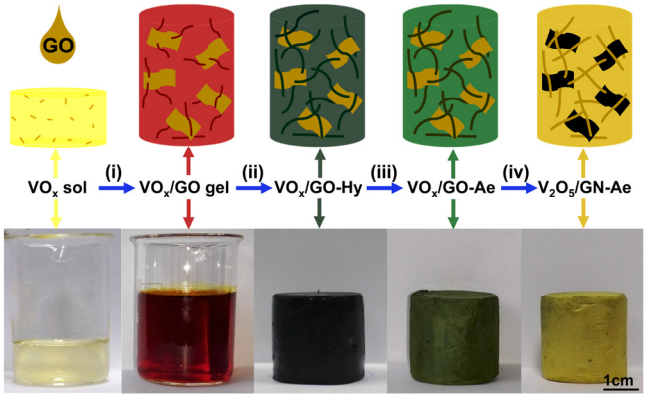


Fig.1 Illustration of the fabrication process and structure of $V_2O_5$/GN hybrid aerogel and corresponding digital images of different formation stages: (i) hydrolysis of $VO_x$ oligomers and self-assembled coordination of $VO_x$ nanofibers and graphene oxide sheets; (ii) ageing of $VO_x$/GO gel and growth of $VO_x$ nanofibers along graphene oxide sheets; (iii) solvent replacement and drying and (iv) thermal reduction of GO, oxidation and partly crystallization of $V_2O_5$.

In-situ growth of $V_2O_5$ nanofibers on surfaces of graphene sheets is difficult to achieve because of the weak interaction between metal oxides and graphene surfaces.[27] However, several functional groups on GO surfaces, such as hydroxyl (–OH), carboxyl (–COOH), and carbonyl (C=O) groups, cause it easier for $VO_x$ nanofibers to grow on GO.[28, 29] Fig. 2 shows that vanadium exhibits a six-fold coordination, which yields an octahedron structure, when the $VO_x$ oligomers hydrolyze; one $H_2O$ molecule in this octahedron structure is opposite the V=O double bond, and an –OH group is present in the equatorial plane.[30] The coordination bonds anchor the $VO_x$ oligomers on the GO sheets. Condensation occurs more rapidly in the x direction because the presence of V–O bonds are not equal in the x and y directions; ribbon-like fibers grow along the graphene sheets.[23] The length and diameter of the fibers increase and gradually interconnect with each other when aging is extended. Thus, a self-assembled and 3D interconnecting porous framework is obtained. The as-prepared hybrid aerogel is mainly supported by the randomly oriented $V_2O_5$ nanowire scaffolds. This result is different from conventional aerogel composite materials with a carbonaceous aerogel skeleton.[31] The $V_2O_5$ is linked with the GO sheets via coordination bonds. Thus, a strong interaction between the $V_2O_5$ and the graphene is observed. Consequently, a stable aerogel structure is formed, which enhanced the performance of the supercapacitors.

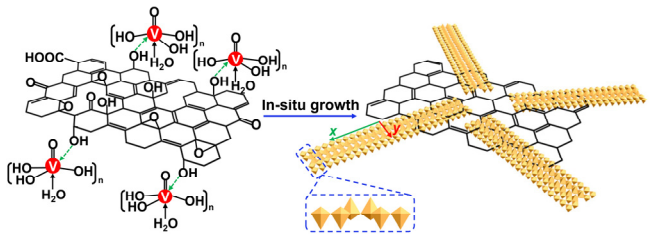


Fig. 2 Schematic of $VO_x$ oligomers growth in situ on graphene oxide sheet. $VO_x$ oligomers incorporate with graphene oxide through coordination with functional groups on the surface of GO at the beginning of hydrolysis. Nanofibers are obtained during the preferred orientation growth of $VO_x$ oligomers.

Figs. 3a, 3d, 3g, and 3j show that the color of the aerogels changed from green ($VO_x$-Ae and $VO_x$/GO-Ae) to yellow ($V_2O_5$-Ae and $V_2O_5$/GN-Ae) when the aerogels are subjected to thermal treatment. This result validates the oxidation of $V^{4+}$.[32] Obviously, the color of the graphene composite aerogels is darker than the $V_2O_5$ aerogels because of the presence of graphene in the graphene composite aerogels. The results of the Fourier transform infrared (FTIR) spectrophotometry and Raman spectroscopy show that the GO is reduced, and a mixture of the $V_2O_5$ and graphene is present in the as-prepared aerogel (Figs. S2 and S3 in ESI†). Moreover, the aerogel exhibits uniform color, which indicates that the $V_2O_5$ and graphene sheets are homogeneously incorporated in the aerogel.

The morphology and structure of the as-prepared aerogels are further investigated by field emission-scanning electron microscopy (FE-SEM), transmission electron microscopy (TEM), and scanning transmission electron microscopy (STEM). Figs. 3b and 3c illustrate that the 3D $VO_x$ architecture is composed of randomly arranged $VO_x$ nanofibers. The curled nanofibers are typically several micrometers long and dozens of nanometers in diameter. The noncrystalline $VO_x$ nanofibers become shorter and straight after the the aerogel is thermally treated because the $V_2O_5$ partly crystallized (Figs. 3e, 3f, and S4 in ESI†). This result corresponds to the result of X-ray diffraction (Fig. S5†). Figs. 3h, 3i, 3k, and 3l strongly confirm that the $V_2O_5$ nanofibers grow along the graphene sheets during

hydrolysis. GO can disperse in water and form a stable dispersion.[33] The $VO_x$ oligomers coordinate with GO at the start of hydrolysis, and a homogeneous 3D structure forms, which benefits from the good dispersity of the GO. The network structure is "frozen" and preserved because of the gelation process; thus, uniform incorporation is observed (Figs. 3m to 3p).

The densities of the $V_2O_5$ aerogel and the $V_2O_5$/GN hybrid aerogel are 26.3 and 27.7 mg $cm^{-3}$, respectively. The weight of the hybrid aerogel is so light that it can be lifted by a feather (Fig. 4a). Fig. 4b shows that the $V_2O_5$/graphene composite aerogel exhibits excellent mechanical property. Moreover, the aerogel is strong enough to support a 100 g weight, which indicates the excellent stability of the 3D aerogel structure.

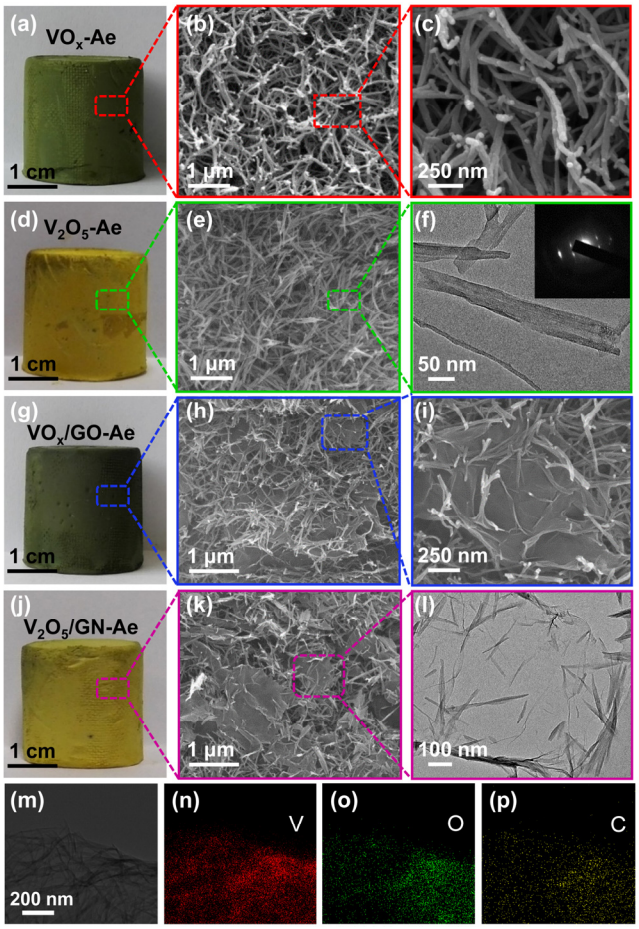


Fig. 3 Morphology and microstructures of aerogel productions. (a-c) Photograph and FESEM images of $VO_x$ aerogel; (d-f) Photograph, FESEM and TEM images of $V_2O_5$ aerogel and SAED patterns of $V_2O_5$ nonofiber (inset in (f)); (g-i) Photograph and FESEM images of $VO_x$/GO composite aerogel; (j-l) Photograph, FESEM and TEM images of $V_2O_5$/GN hybrid aerogel and (m) STEM image of $V_2O_5$/GN hybrid aerogel and corresponding elemental mapping images of (n) vanadium, (o) oxygen, and (p) carbon, indicating the homogeneous dispersion of V, O, and C in the hybrid aerogel.

The pore structure of the $V_2O_5$/graphene composite aerogel is investigated by nitrogen adsorption–desorption measurements. Fig. 4c shows that the adsorption–desorption curves exhibit type-IV adsorption hysteresis loops. This finding indicates that the structure is mesoporous.[34] Furthermore, the pore size distribution of the aerogel, which is calculated by the Barret–Joyner–Halenda (BJH) method, ranges from 1 nm to 100 nm. This result demonstrates that the composite aerogel exhibits hierarchical macro-, meso-, and microporous structures (inset in Fig. 4c). The macropores can act as a bulk buffering reservoir for electrolytes to minimize diffusion distances to interior surfaces.[35] The mesopores provide a large accessible surface area for ion transport/charge storage, and micropores strengthen the electric double layer capacitance.[36, 37] Brunauer–Emmett–Teller (BET) analysis reveals that the specific surface area and total pore volume of the $V_2O_5$/graphene hybrid aerogel are 172 $m^2$ $g^{-1}$ and 0.53 $cm^3$ $g^{-1}$. These values are higher than those of the as-prepared $V_2O_5$ aerogel (60 $m^2$ $g^{-1}$ and 0.15 $cm^3$ $g^{-1}$, respectively). The surface area of the $V_2O_5$/graphene hybrid aerogel is also higher compared with those of the 3D $V_2O_5$ architecture (133 $m^2$ $g^{-1}$),[21] $V_2O_5$/graphene composite (64 $m^2$ $g^{-1}$),[38] graphene/$Fe_3O_4$ nanoparticle aerogel (95.22 $m^2$ $g^{-1}$),[31] and $MnO_2$ nanowire/graphene composite (107 $m^2$ $g^{-1}$).[39]

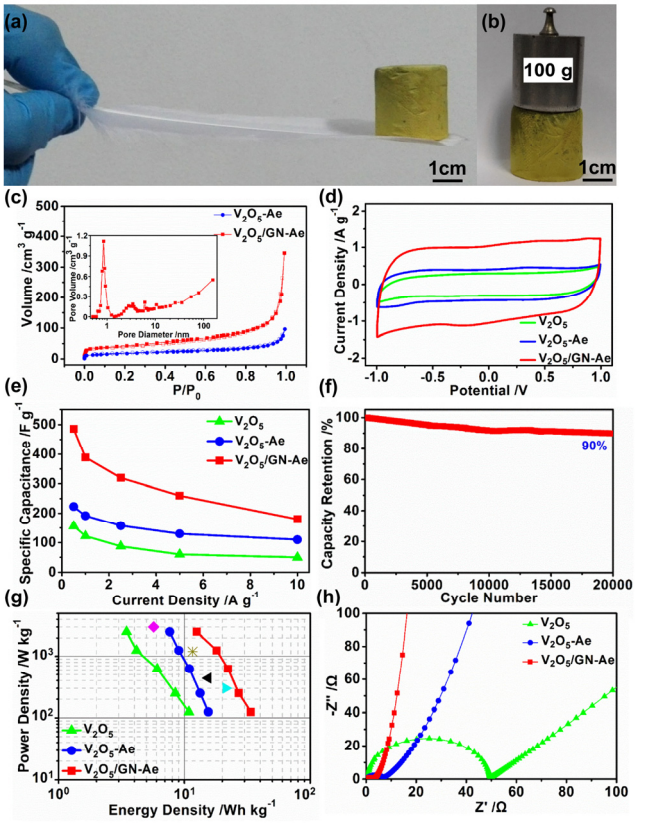


Fig. 4 (a) Lightweight $V_2O_5$/GN hybrid aerogel standing on a feather; (b) Obtained strong $V_2O_5$/GN composite aerogel supporting the weight; (c) Nitrogen adsorption/desorption isotherms of $V_2O_5$ aerogel and $V_2O_5$/GN hybrid aerogel and corresponding Barrett-Joyner-Halenda (BJH) pore-size distribution (inset); (d) Cyclic voltammetry (CV) curves of $V_2O_5$ powder, $V_2O_5$ aerogel and $V_2O_5$/GN hybrid aerogel at a scan rate of 5 mV $s^{-1}$ in the range of -1 to 1 V in 1 M $Na_2SO_4$ aqueous solution; (e) Specific capacitance as a function of current density for $V_2O_5$ powder, $V_2O_5$ aerogel and $V_2O_5$/GN composite aerogel; (f) Cycling stability of supercapacitor with $V_2O_5$/GN composite aerogel electrodes at 10 A $g^{-1}$ in 1 M $Na_2SO_4$ electrolyte; (g) Ragone plots of supercapacitors based on $V_2O_5$ powder, $V_2O_5$ aerogel and $V_2O_5$/GN hybrid aerogel electrodes

in comparison with graphene hydrogel electrodes(◊, ref. 41), $V_2O_5$ nanotube electrodes (*, ref. 42), graphene/$VO_2$ nanobelt composite electrodes(►, ref. 43)and $MnO_2$ nanorod/graphene-$V_2O_5$ nanowire/graphene hybrid electrodes(◄, ref. 44) and (h) Electrochemical impedance spectra (EIS) of raw $V_2O_5$ powder, $V_2O_5$ aerogel and $V_2O_5$/GN aerogel composite.

The unique hierarchical porous structure of the $V_2O_5$/graphene hybrid aerogel makes it an excellent candidate in energy storage. We evaluated the electrochemical behavior of the $V_2O_5$/graphene hybrid aerogel as electrodes of supercapacitors in symmetric two-electrode cells using 1 M $Na_2SO_4$ aqueous solution as electrolyte. For comparison, the electrochemical properties of $V_2O_5$ aerogel and raw $V_2O_5$ powder were also tested under the same conditions and the results are shown in Fig. 4d. The nearly rectangular cyclic voltammetry (CV) curve and redox peaks of the $V_2O_5$/graphene hybrid aerogel indicate the synergistic effect of the electrochemical double layer capacitors and pseudocapacitors.[40] We also measured the galvanostatic charge/discharge behaviors of the $V_2O_5$/graphene hybrid aerogel at various current densities from 0.5 A $g^{-1}$ to 10 A $g^{-1}$ to understand the high electrochemical performance of the aerogel. Fig. 4e shows the results of the test conducted. The specific capacitance of the $V_2O_5$/graphene composite aerogel is 486 F $g^{-1}$ at a current density of 0.5 A $g^{-1}$. The obtained specific capacitance is much higher than the $V_2O_5$ aerogel (233 F $g^{-1}$) and raw $V_2O_5$ (157 F $g^{-1}$) (Figs. S6–8 in ESI†).

The cycle stability of the 3D hybrid aerogel is also evaluated at a constant current density of 10 A $g^{-1}$. Fig. 4f shows that the $V_2O_5$/graphene hybrid aerogel exhibits excellent cycling performance even after 20000 charge–discharge cycles, and 90% of the specific capacitance is retained, which is comparable to EDLCs. Fig. 4g compares the energy density and power density derived from the galvanostatic charge/discharge characteristics of different prototype supercapacitors. Remarkably, the $V_2O_5$/graphene hybrid aerogel exhibits a high energy density of 68 Wh $kg^{-1}$ at a power density of 250 W $kg^{-1}$. This result indicates the outstanding high-energy performance of the $V_2O_5$/graphene hybrid aerogel. The enhanced specific capacitance, high power and energy densities, and long cycle life of the hybrid aerogel electrode is attributed to the unique hierarchical porous structure of the hybrid aerogel. The interconnected network of the $V_2O_5$ can shorten diffusion distances from external electrolytes to interior surfaces and improve ion accessibility in the 3D framework. The graphene sheets within the hybrid aerogel can serve as multi-dimensional pathways to transport electrons and reduce charge transfer resistance (Fig. 4h). Finally, the combined EDLCs and pseudocapacitors can simultaneously increase specific capacitance and cycling stability.[5, 31, 45]

## Conclusions

In summary, we successfully fabricated a $V_2O_5$/graphene hybrid aerogel at ambient pressure through a simple sol-gel method from commercial $V_2O_5$ powder for the first time. The $V_2O_5$ nanofibers are anchored and *in-situ* grown on the graphene surfaces through coordination effect. Thus, a homogeneous and stable hybrid aerogel structure formed. The fabricated 3D hybrid aerogel exhibits low density(27.7mg $cm^{-3}$), large specific surface area (172 $m^2$ $g^{-1}$), and favorable mechanical strength. Moreover, the 3D hybrid aerogel displays hierarchical macro-, meso-, and microporous structures. In addition, the $V_2O_5$/GN-Ae-based supercapacitor exhibits enhanced specific capacitance (486 F $g^{-1}$), high energy density (68 Wh $kg^{-1}$) and long cycle life (> 20000 cycles). These effects are caused by the hierarchical porous structure of the aerogel. We believe that the fabricated 3D $V_2O_5$/graphene hybrid aerogel can be used in broad applications, such as lithium ion batteries, sensors, electronics, analysis, and adsorbents, because of the unique structure of these aerogels.

## Acknowledgements

The authors gratefully acknowledge the financial supports by Shanghai Committee of Science and Technology (11nm0501300 and 13JC1408700), National Natural Science Foundation of China (51472182, 51272179 and 51102183) and National High-Tech R-D Program of China (863 Program) (2013AA031801).

## Notes and references

Shanghai Key Laboratory of Special Artificial Microstructure, Tongji University, Shanghai, 200092, China. E-mail: gao@tongji.edu.cn; wugm@tongji.edu.cn

† Electronic Supplementary Information (ESI) available: Experimental details, supplementary figures and discussions. See DOI: 10.1039/c000000x/

1 D. Pech, M. Brunet, H. Durou, P. H. Huang, V. Mochalin, Y.Gogotsi, P.-L. Taberna and P. Simon, *Nat. Nanotechnol.*, 2010, **5**, 651.
2 M. F. El-Kady, V. Strong, S. Dubin and R. B. Kaner, *Science*, 2012, **335**, 1326.
3 X. Lang, A. Hirata, T. Fujita and M. W. Chen, *Nat. Nano.*, 2011, **6**, 232.
4 Y. W. Zhu, S. Murali, M. D. Stoller, K. J. Ganesh, W. W. Cai, P. J. Ferreira, A. Pirkle, R. M. Wallace, K. A. Cychosz, M. Thommes, D. Su, E. A. Stach and R. S. Ruoff, *Science*, 2011, **332**, 1537.
5 P. Simon1 and Y. Gogotsi, *Nat. Mater.*, 2008, **7**, 845.
6 J. Biener, M. Stadermann, M. Suss, M. A. Worsley, M. M. Biener, K. A. Rose and T. F. Baumann, *Energy Environ. Sci.*, 2011, **4**, 656.
7 S. Nardecchia, D. Carriazo, M. L. Ferrer, M. C. Gutiérrez and F. del Monte, *Chem. Soc. Rev.*, 2013, **42**, 794.
8 M. A. Worsley, S. O. Kucheyev, J. D. Kuntz, T. Y. Olson, T. Y.-J. Han, A. V. Hamza, J. H. Satcher, Jr. and T. F. Baumann, *Chem. Mater.*, 2011, **23**, 3054.
9 X. T. Zhang, Z. Y. Sui, B. Xu, S. F. Yue, Y. J. Luo, W. C. Zhan and B. Liu, *J. Mater. Chem.*, 2011, **21**, 6494.
10 Z. Y. Sui, Q. H. Meng, X. T. Zhang, Rui Ma and Bing Cao, *J. Mater. Chem.*, 2012, **22**, 8767.
11 H. Huang, P. W. Chen, X. T. Zhang, Y. Lu and W. C. Zhan, *Small*, 2013, **9**, 1397.
12 X. Y. Wang, L. Liu, X. Y. Wang, L. H. Yi, C. Y. Hu and X. Y. Zhang, *Mater. Sci. Eng. B*, 2011, **176**, 1232.
13 X. Y. Wang, X. Y. Wang, L. H. Yi, L. Liu, Y. Z. Dai and H. Wu, *J. Power Sources*, 2013, **224**, 317.

14 M. X. Chen, H. Wang, L. Z. Li, Z. Zhang, C. Wang, Y. Liu, W. Wang and J. P. Gao, *ACS Appl. Mater. Interfaces*, 2014, **6**, 14327.
15 S. S. Wu, W. F. Chen and L. F. Yan, *J. Mater. Chem. A*, 2014, **2**, 2765.
16 J. Cai, S. L. Liu, J. Feng, S. Kimura, M. Wada, S. Kuga and L. N. Zhang, *Angew. Chem. Int. Ed.*, 2012, **124**, 2118.
17 L. Chen, B. Wei, X. T. Zhang and C. Li, *Small*, 2013, **9**, 2331.
18 Z. Q. Niu, L. L. Liu, L. Zhang, Q. Shao, W. Y. Zhou, X. D. Chen and S. S. Xie, *Adv. Mater.*, 2014, **26**, 3681.
19 H. J. Yin, S. L. Zhao, J. W. Wan, H. J. Tang, L. Chang, L. C. He, H. J. Zhao, Y. Gao and Z. Y. Tang, *Adv. Mater.*, 2013, **25**, 6270.
20 L. Xiao, D. Q. Wu, S. Han, Y. S. Huang, S. Li, M. Z. He, F. Zhang and X. L. Feng, *ACS Appl. Mater. Interfaces*, 2013, **5**, 3764.
21 J. X. Zhu, L. J. Cao, Y. S. Wu, Y. J. Gong, Z. Liu, H. E. Hoster, Y. H. Zhang, S. T. Zhang, S. B. Yang, Q. Y. Yan, P. M. Ajayan and R. Vajtai, *Nano Lett.*, 2013, **13**, 5408.
22 M. K. Atal, V. Dhayal, M. Nagar, R. Bohra, K. S. Rathore and N. S. Saxena, *J. Sol-Gel Sci. Technol.*, 2010, **53**, 67.
23 J. Livage, *Chem. Mater.*, 1991, **3**, 578.
24 O. Pelletier, P. Davidson, C. Bourgaux, C. Coulon, S. Regnault and J. Livage, *Langmuir*, 2000, **16**, 52953.
25 J. Livage, *Solid State Ionics*, 1996, **86**, 935.
26 Z.-L. Wang, D. Xu, Y. Huang, Z. Wu, L.-M. Wang and X.-B. Zhang, *Chem. Commun.*, 2012, **48**, 976.
27 S. Li, D. Q. Wu, C. Cheng, J. Z. Wang, F. Zhang, Y. Z. Su and X. L. Feng, *Angew. Chem. Int. Ed.*, 2013, **125**, 12327.
28 K. P. Loh, Q. L. Bao, G. Eda and M. Chhowalla, *Nat. Chem.*, 2010. **2**, 1015.
29 S. J. Park and R. S. Ruoff, *Nat. Nanotechnol.*, 2009, **4**, 217.
30 M. Sathiya, A. S. Prakash, K. Ramesha, J-M. Tarascon and A. K. Shukla, *J. Am. Chem. Soc.*, 2011, **133**, 16291.
31 W. F. Chen, S. R. Li, C. H. Chen and L. F. Yan, *Adv. Mater.*, 2011, **23**, 5679.
32 N. S. Chandrappa and J. Livage, *Nature*, 2002, 416.
33 D. Li, M. B. Müller, S. Gilje, R. B. Kaner and G. G. Wallace, *Nat. Nanotechnol.*, 2008, **3**, 101.
34 Z.-S. Wu, Y. Sun, Y.-Z. Tan, S. B. Yang, X. L. Feng and K. Müllen, *J. Am. Chem. Soc.*, 2012, **134**, 19532.
35 A. Vu, Y. Qian, A. Stein, *Adv. Energy Mater.* 2012, **2**, 1056.
36 T.-Y. Wei, C.-H. Chen, H.-C. Chien, S.-Y. Lu and C.-C. Hu, *Adv. Mater*., 2010, **22**, 347.
37 J. C. Lytle, J. M. Wallace, M. B. Sassin, A. J. Barrow, J. W. Long, J. L. Dysart, C. H. Renninger, M. P. Saunders, N. L. Brandella and D. R. Rolison, *Energy Environ. Sci.*, 2011, **4**, 1913.
38 H. B. Zhao, L. Y. Pan, S. Y. Xing, J. Luo and J. Q. Xu, *J. Power Sources*, 2013, **222**, 21.
39 Z.-S. Wu, W. C. Ren, D.-W. Wang, F. Li, B. L. Liu and H.-M. Cheng, *ACS Nano*, 2010, **4**, 5835.
40 J. T. Zhang, J. W. Jiang, H. L. Li and X. S. Zhao, *Energy Environ. Sci.*, 2011, **4**, 4009.
41 L. Zhang and G. Q. Shi, *J. Phys. Chem. C*, 2011, **115**, 17206.
42 S. D. Perera, B. Patel, J. Bonso, M. Grunewald, J. P. Ferraris and K. J. Balkus, Jr. *ACS Appl. Mater. Interfaces*, 2011, **3**, 4512.
43 H. W. Wang, H. Yi, X. Chen and X. F. Wang, *J. Mater. Chem. A*, 2014, **2**, 1165.
44 S. D. Perera, M. Rudolph, R. G. Mariano, N. Nijem, J. P. Ferraris, Y. J. Chabal and K. J. Balkus, Jr. *Nano Energy*, 2013, **2**, 966.
45 D.-W. Wang, F. Li, M. Liu, G. Q. Lu and H.-M. Cheng, *Angew. Chem. Int. Ed.*, 2008, **47**, 373.

A self-assembled three-dimensional hierarchical porous $V_2O_5$/graphene hybrid aerogel for high-performance supercapacitor.